Hybrid Phase at the Quantum Melting of the Wigner Crystal

Houman Falakshahi and Xavier Waintal

Nanoelectronic Group, Service de Physique de l'Etat Condensé, CEA Saclay F-91191 Gif-sur-Yvette Cedex, France

(Received 24 June 2004; published 31 January 2005)

We study the quantum melting of the two-dimensional Wigner crystal using a fixed node quantum Monte Carlo approach. In addition to the two already known phases (Fermi liquid at large density and Wigner crystal at low density), we find a third stable phase at intermediate values of the density. The third phase has hybrid behaviors in between a liquid and a solid. This hybrid phase has the nodal structure of a Slater determinant constructed out of the bands of a triangular lattice.

DOI: 10.1103/PhysRevLett.94.046801 PACS numbers: 73.20.Qt, 02.70.Ss, 71.10.Ca

The physics of a system of N electrons confined on a two-dimensional surface S is a textbook problem at the root of a very large body of literature. Two competing energies, electrostatic and kinetic, give rise to a rich phase diagram. The physics is controlled by the dimensionless parameter $r_s = m^* e^2/(\hbar^2 \epsilon \sqrt{\pi n})$ which is the ratio of the average distance between electrons over the effective Bohr radius (e is the electronic charge, ϵ the dielectric constant, m^* the effective mass, and $n = N/S$ the electronic density). At large density (low r_s), the kinetic energy dominates and the system is in a Fermi liquid phase [1]. Since the work of Wigner [2] in 1934, it is also known that, at low density (large r_s), the Coulomb repulsion dominates and the electrons crystallize onto a (Wigner) triangular crystal [2,3]. In their pioneering work in 1989, Tanatar and Ceperley [4] were able to locate that the quantum melting of the crystal occurs for a critical value of $r_s \approx 37 \pm 5$. Their work, which used a fixed node quantum Monte Carlo [5] (FN-QMC) technique, was followed by more precise numerics [6] and a better description of the liquid phase [7,8] that included backflow corrections.

This simple picture of a, presumably first order, direct transition between the solid and the liquid phase is to be contrasted with other aspects of the physics of the Wigner crystal which show more complex behaviors. For instance, its magnetism is believed to include a spin liquid phase in addition to the ferromagnetic phase found at very large r_s [9]. The fermionic statistics of the electrons is also known to play a crucial role for $r_s \leq 60$, where the melting of the bosonic Wigner crystal occurs [10]. Also, the classical melting [11–13] (as a function of temperature) occurs in two steps. The system first loses its translational order but retains some orientational order (hexatic phase [13]), while at higher temperature all order disappears. The classical melting has been studied on electrons on a helium surface [14] (where the additional coupling to the helium degrees of freedom gives rise to interesting physics) as well as in semiconductor heterostructures in a high magnetic field [11]. The possibility that the quantum melting of a crystal would also take place in two steps, leading to a highly correlated intermediate phase, had been discussed as early as 1969 by Andreev and Lifshitz [15], who proposed that a liquid of defects would exist together with the crystal state. This proposal has been revisited recently in small systems using exact diagonalization techniques [16]. Another interesting proposal includes the possibility of having bubbles or stripes of one phase inside the other [17].

In this Letter, we study a new phase which is a hybrid of a liquid and a solid using a FN-QMC technique similar to the one used in [4]. The FN-QMC approach is a very powerful tool to tackle this problem, but it is of primary importance to understand the nature of the approximations which it involves. The method lies halfway between a black box and a variational approach. Technically, the FN-QMC algorithm is fed with a wave function, called the *guiding wave function* (GWF), that has to be given explicitly, and that should be close to the ground state of the system. The FN-QMC algorithm modifies the GWF to become as close as possible to the ground state of the system, given the constraint that the sign of the wave function remains unchanged at every point of the Hilbert space. The method gives the best wave function for a given structure of the nodes of the GWF and is in this sense variational [18]. Our main result is summarized in the stability diagram, Fig. 1, where the energies of the different phases (i.e., associated with the different GWFs) are plotted as a function of r_s. The hybrid phase is found to be stable in the (critical) region $r_s^* < r_s < r_s^{**}$ with $r_s^* \approx 30$ and $r_s^{**} \approx 80$.

Model.—We consider a system of N spinless electrons on a square $L_x \times L_y$ grid with periodic boundary conditions whose Hamiltonian is given by

$$H = -t \sum_{\langle \vec{r}, \vec{r}' \rangle} c_{\vec{r}}^\dagger c_{\vec{r}'} + \frac{U}{2} \sum_{\vec{r} \neq \vec{r}'} V(\vec{r} - \vec{r}') n_{\vec{r}} n_{\vec{r}'} + \lambda. \quad (1)$$

The operator $c_{\vec{r}}^\dagger$ ($c_{\vec{r}}$) creates (destroys) an electron on point $\vec{r}$ with the standard anticommutation relation rules. The sum $\sum_{\langle \vec{r}, \vec{r}' \rangle}$ is done on the nearest neighbor points on the grid and t is the corresponding hopping amplitude. The density operator reads $n_{\vec{r}} = c_{\vec{r}}^\dagger c_{\vec{r}}$. U is the effective strength of the interaction. The two-body interaction $V(\vec{r})$ is obtained from the bare Coulomb interaction using the Ewald summation techniques to avoid finite size effects, and reads

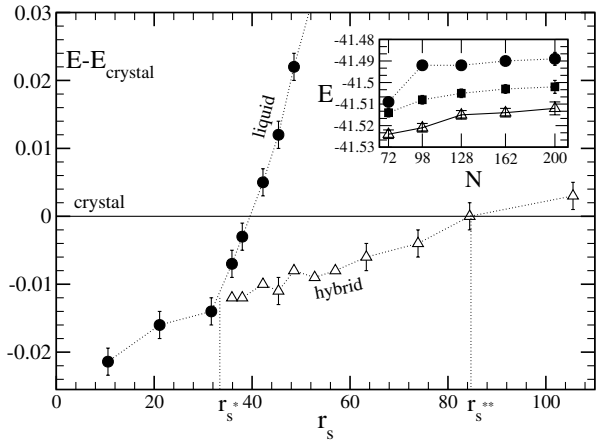

FIG. 1. Energy difference $E_{\text{liquid}} - E_{\text{crystal}}$ (circles) and $E_{\text{hybrid}} - E_{\text{crystal}}$ (triangles) as a function of r_s for 72 electrons in a 48×84 grid. Inset: energies of the three phases at $\nu = 1/56$ and $U = 20$ ($r_s \approx 42.2$) as a function of the number of particles up to 200 electrons in a 80×140 grid. From top to bottom: liquid, crystal, and hybrid phase. Energies are in units of $2\pi N\nu t$.

$V(\vec{r}) = \sum_{\vec{L}} \frac{1}{|\vec{r}+\vec{L}|}\text{Erfc}(k_c|\vec{r}+\vec{L}|) + \frac{2\pi}{L_x L_y}\sum_{\vec{K}\neq\vec{0}} \frac{1}{|\vec{K}|}\text{Erfc}[|\vec{K}|/(2k_c)]\cos(\vec{K}\cdot\vec{r})$. In the previous equation, k_c is a (irrelevant) cutoff. The vector $\vec{L}$ takes discrete values $\vec{L} = (n_x L_x, n_y L_y)$ with n_x and n_y integer numbers. The vector $\vec{K}$ also takes discrete values, $\vec{K} = (\frac{2\pi}{L_x}n_x, \frac{2\pi}{L_y}n_y)$ and $(n_x, n_y) \neq (0,0)$. The complementary error function is $\text{Erfc}(r) = \frac{2}{\sqrt{\pi}} \times \int_x^\infty e^{-t^2} dt$. In order to assure electrostatic neutrality, we add a positive continuous background $\lambda/N = 4t + U\tilde{V}(\vec{0}) - 2U\nu\sqrt{\pi}/k_c - 2Uk_c/\sqrt{\pi}$, where $\nu = \frac{N}{L_x L_y}$ is the average electronic density and $\tilde{V}(\vec{r}) = V(\vec{r})$ with the restriction that the sum over $\vec{L}$ does not includes the null vector. The jellium allows us to make contact with the continuous model at low filling factor. However, it is merely a constant term, and the phase diagram cannot depend on its presence in any way. All energies in the problem are measured in units of $2\pi N\nu t$. The r_s parameter for this model reads $r_s = U/(2t\sqrt{\pi\nu})$. In our numerics we have used $\nu = 1/56$ and $\nu = 1/780$. Standard two-dimensional gas in GaAs heterostructures where the underlying grid is given by the Ga and As atoms corresponds to $\nu \approx 1/1000$ or $\nu \approx 1/10\,000$ for the most diluted ones. For these filling factors, only the bottom of the one-body band is filled, and the noninteracting dispersion relation is almost parabolic (in both real 2D gas and our tight-biding model). Formally, Eq. (1) tends toward the continuous model studied in Ref. [4] when $\nu \ll 1$ (provided our energies are multiplied by $2/r_s^2$). In order for the Wigner crystal to fit into the system without distortion, we chose $L_y \approx \sqrt{3}L_x$ and $N = 2P^2$ with P integer. The electrons in our study are fully spin polarized, which corresponds to a system with a strong in-plane magnetic field. However, our results also extend to zero field systems since at $r_s \geq 20$ the polarized fluid is more stable than the nonpolarized one [6,7]. Last, we have added a very small disorder $\sum_{\vec{r}} v_{\vec{r}} n_{\vec{r}}$ in order to lift the degeneracies of the noninteracting problem. $v_{\vec{r}}$ are independent and uniformly distributed inside $[-W/2, +W/2]$. We choose $W = 10^{-3}$ corresponding to an extremely large ratio $l/\lambda_F \sim 10^7$ of the mean-free path l over Fermi wavelength λ_F. We explicitly checked that our results are insensitive to the presence of this disorder.

FN-QMC Method.—The operator e^{-Ht} is applied stochastically to an initial GWF in order to project it to the exact ground state. Our implementation is based on the Green function Monte Carlo algorithm for lattice Hamiltonians introduced in [19]. Important sampling [20] and fixed node (FN) are implemented as in [18] by replacing H by an effective Hamiltonian H_{FN} that depends on the GWF. H_{FN} forbids the sign of the wave function to change. The energies calculated with H_{FN} are larger than the one of the true ground state but smaller than the variational energy associated with the guiding wave function [18]. At $\nu \ll 1$, the technique is equivalent to the continuous fixed node diffusive Monte Carlo algorithm used in [4]. The algorithm to update the Slater determinants can be found in [21]. By sampling directly the time spent by the walkers at one point of the Hilbert space using the algorithm described in [19], we can use arbitrary small time steps and effectively work in continuous (imaginary) time. Instead of using branching, the control of the walkers population is done using a fixed number of walkers and the reconfiguration algorithm introduced by Sorella [22]. This algorithm allows one to avoid the bias introduced in the branching technique by artificially controlling the walker population. Quantum averages of physical quantities $\langle \cdots \rangle$ are calculated using the forward walking technique [22], and hence do not suffer from the bias of mixed estimates. A typical point for 72 particles involves 20 independent Monte Carlo runs with 5000 walkers each.

Guiding Wave Functions.—The GWFs used in our calculations are Slater determinants multiplied by Jastrow functions,

$$\Psi(\vec{r}_1, \vec{r}_2, \ldots, \vec{r}_N) = \text{Det}[\phi_i(\vec{r}_j)]\prod_{i<j} J(|\vec{r}_i - \vec{r}_j|). \quad (2)$$

The Jastrow part takes Coulomb interaction into account by introducing correlations between electrons. It has no nodes, and thus is irrelevant in the FN-QMC results. We use modified Yukawa functions [23], $J(r) = \exp[\frac{qA(r_s)}{r} \times (1 - e^{-B(r_s)r/a})]$, where $a = 1/\sqrt{\pi\nu}$ is the average distance between electrons. $A(r_s)$ and $B(r_s)$ are (optimized) variational parameters. We checked that the FN-QMC results are not sensitive to the choice of the Jastrow function. The Slater determinant of one-body wave functions, $\text{Det}[\phi_i(\vec{r}_j)]$ enforces the antisymmetric nature of the fermionic wave function and is responsible for the nodal structure of the GWF. The GWFs used in the literature are constructed out of plane waves $\phi_i(\vec{r}_j) \propto e^{i\vec{k}_i\cdot\vec{r}_j}$ for the liquid GWF Ψ_{liq} [in practice, the plane waves are obtained by diagonalizing Eq. (1) with $U = 0$]. For the crystal GWF

$\Psi_{\rm cry}$, localized orbitals $\phi_i(\vec{r}_j) \propto e^{-(\vec{r}_j-\vec{u}_i)^2/d_0^2}$ are used. Here the $\vec{u}_i$ with $i \in \{1 \ldots N\}$ stand for the positions of the electrons in the classical crystal and $d_0 \propto a$ is a variational parameter. $\Psi_{\rm liq}$ ($\Psi_{\rm cry}$) provides the exact ground state of H at very large (low) density.

Hybrid GWF.—Below we give the detailed construction of a new GWF, $\Psi_{\rm hyb}$, such that the $\phi_i(\vec{r}_j)$ are the Bloch states of a triangular crystal. First, an effective one-body Hamiltonian $H_{\rm eff}$ is constructed for an effective hole in a periodic potential given by a classical Wigner crystal,

$$H_{\rm eff} = -t \sum_{\langle \vec{r},\vec{r}' \rangle} c^\dagger_{\vec{r}} c_{\vec{r}'} - U^* \sum_{\vec{r}} W(\vec{r}) n_{\vec{r}}, \qquad (3)$$

where the one-body potential is $W(\vec{r}) = \sum_{i=1}^{N} V(\vec{r} - \vec{u}_i)$. The singularity of $W(\vec{r})$ at $\vec{r} = \vec{u}_i$ has been removed by setting $W(\vec{u}_i) \equiv W[\vec{u}_i + (1,0)]$, and we checked that our results are unaffected by this choice. In a second step, we take advantage of the presence of the underlying grid and $H_{\rm eff}$ is numerically diagonalized using Lanczos algorithm. The N orbitals of lowest energy $\phi_i(\vec{r})$ ($1 \le i \le N$) are then used to construct the Slater determinant. U^* is a variational parameter.

The underlying idea behind the construction of $\Psi_{\rm hyb}$ is to put on the same level the melting of the Wigner crystal in real space (as the density is increased) and the destruction of the Fermi sea in momentum space (as the density is decreased). $\Psi_{\rm hyb}$ allows for an interpolation between momentum space ($U^* = 0$) and real space ($U^* \gg 1$). The available values of momentum $\vec{k}$ are taken within the first Brillouin zone, and hence, the liquid-hybrid transition can be viewed as an instability of the shape of the Fermi surface that goes from a circular to a hexagonal form. The symmetry is broken at this transition, but it is only in a second step that larger values of $|\vec{k}|$ will come into play, allowing the $\phi_i(\vec{r}_j)$ to get localized and the actual crystallization to take place. This transition in two steps, where first the direction of $\vec{k}$ and second its absolute value are affected, is reminiscent of the hexatic phase predicted in the classical melting.

Stability of the Hybrid Phase.—Figure 1 shows the energy differences $E_{\rm liq} - E_{\rm cry}$ and $E_{\rm hyb} - E_{\rm cry}$ as a function of r_s for a system of 72 electrons in a 48×84 grid. These energy differences are very small, less than 0.1% of the total energy of the system. $r_s \approx 40$, where $E_{\rm liq} - E_{\rm cry} \approx 0$ would be the critical value or r_s in the absence of the hybrid phase [4]. However, we find that, for $30 < r_s < 80$, the hybrid phase has a smaller energy than both the liquid and the solid phase. Around $r_s^* \approx 30$ we find a jump of U^* from zero to $U^* = 0.3$ [a value which corresponds to the splitting of the lowest energy band of Eq. (3)]; see the inset of Fig. 2. $U^*/U \approx 0.015$ up to $r_s^{**} \approx 80$, above which the crystal phase becomes more stable than the hybrid phase. Finite N corrections shown in the inset of Fig. 1 at $r_s \approx 42.2$ are of the order of ~ 0.01 but keep the energy differences almost invariant. We note that although the variational energy of the hybrid phase is lower than the one of the liquid it is still higher than the crystal variational energy. The FN-QMC treatment is necessary to show the stability of the hybrid phase, as shown in Fig. 2. To make contact with the calculations of [4,6], we have repeated these calculations for a more diluted system $\nu = 1/780$, where the role of the underlying grid is negligible. The results are plotted in Fig. 3 in the same way as Fig. 2 of [4] (with the Madelung constant $c_1 = -2.2122$). In the inset of Fig. 3 we have reported the Wigner crystal data of [4,6] for comparison and find a good quantitative agreement with the latter (finite size corrections between system with 72 and 56 particles are of the order of the size of the

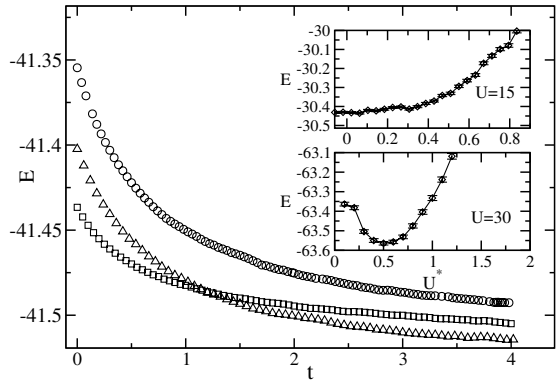

FIG. 2. Energy of the liquid (circle, $A = 6.0$, $B = 2.25$), hybrid (triangle, $A = 4.9$, $B = 2.58$, $U^* = 0.3$), and crystal (square, $A = 4.9$, $B = 2.5$, $d_0 = 2.95$) phases as a function of imaginary time t for 72 electrons in a 48×84 grid at $U = 20$ ($r_s \approx 42.2$). Inset: variational energy of the hybrid phase as a function of U^* at $U = 15$ ($r_s \approx 31.67$ upper panel, $A = 4.7$, $B = 2.3$) and $U = 30$ ($r_s \approx 63.33$ lower panel, $A = 5.7$, $B = 2.9$). Energies are in units of $2\pi N \nu t$.

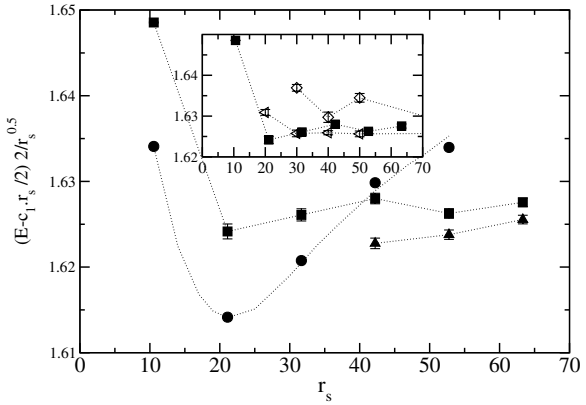

FIG. 3. $[2E(r_s) - c_1 r_s]/r_s^{1/2}$ as a function of r_s for 72 electrons in a 180×312 grid. The curves for the liquid (circles), crystal (squares), and hybrid phases (triangle) can be compared directly with Fig. 2 of [4]. Inset: Comparison of our result with previous calculations for the crystal phase. $[2E(r_s) - c_1 r_s]/r_s^{1/2}$ is plotted as a function of r_s. The curves show our data for 72 electrons in a 180×312 grid (squares), the data of Ref. [4] for 56 electrons (diamonds), and the more recent data of Ref. [6] for 56 electrons (triangles).

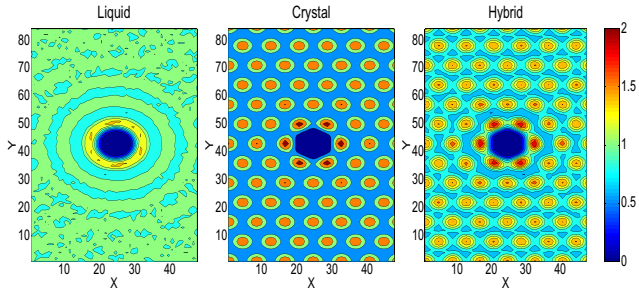

FIG. 4 (color online). Density-density correlation function for a system of 72 electrons in a 48×84 grid. $g(\vec{r})$ measures the probability of finding a particle in (X, Y), knowing that one electron lies in the middle of the sample. From left to right, the liquid, crystal, and hybrid phases are represented at $U = 20$ ($r_s \approx 42.2$).

symbols and favor the smallest systems, see inset of Fig. 1). We note that, around $r_s = 40$, the energy difference between the liquid and the hybrid phase (~ 0.01) is about three times as big as the energy that could be gained on the liquid phase using backflow corrections (~ 0.0037 at $r_s = 30$ in [7]).

Nature of the Hybrid Phase.—It is important to realize that, as described above, the nature of the intermediate phase is by construction something hybrid, being made of (delocalized) Bloch waves, yet having already the symmetry of the Wigner crystal. More insight can be gained by computing the electronic density $\langle n_{\vec{r}} \rangle$ (not shown) which is the superposition of peaks at the classical positions (the $\vec{u}_i$) of the electrons in the crystal over a small background. At $r_s = 42$, the background is found to contain approximately 35% of the electrons while the rest lies in the peaks of the crystal. This amount is stable upon increasing N up to $N = 200$. Although the total energy of the hybrid phase is below those of the liquid and crystal, both its kinetic and electrostatic energies lie in between those of the liquid and solid. Figure 4 shows the density-density correlation function (roughly measuring the probability of finding an electron at point $\vec{r}$ knowing that an electron is at point $\vec{0}$), $g(\vec{r}) = \frac{L_x L_y}{N(N-1)} \langle c^\dagger_{\vec{r}} c^\dagger_{\vec{0}} c_{\vec{0}} c_{\vec{r}} \rangle$ for the three phases. $g_{\mathrm{hyb}}(\vec{r})$ for the hybrid phase is intermediate between a liquid and a crystal. The value of $g_{\mathrm{hyb}}(\vec{r})$ at its peaks is only twice as big as in the valley to be compared to a factor 15 at $r_s = 100$. In fact a very good fit is obtained with $g_{\mathrm{hyb}}(\vec{r}) \approx 0.35 g_{\mathrm{liq}}(\vec{r}) + 0.65 g_{\mathrm{cry}}(\vec{r})$. Upon increasing r_s, the percentage of the background decreases smoothly ($\sim 25\%$ at $r_s = 50$, $\sim 10\%$ at $r_s = 60$). We conclude by noting that, while a symmetry is broken at the liquid-hybrid transition (therefore establishing it as a phase transition), no such thing exists when the system goes from the hybrid phase to the crystal one. Hence, the two phases are somehow on the same footing as a gas and a liquid, and it is not clear at this moment whether there is a crossover or a phase transition between one and the other.

We are grateful to D. L'Hôte, P. Roche, J. Segala, and F. I. B. Williams for useful discussions. We give special thanks to J.-L. Pichard to whom we are indebted for many stimulating discussions.

[1] D. Pines and P. Nozieres, *Theory of Quantum Liquids* (Benjamin, New York, 1966), Vol. I.
[2] E. P. Wigner, Phys. Rev. **46**, 1002 (1934).
[3] L. Bonsall and A. A. Maradudin, Phys. Rev. B **15**, 1959 (1977).
[4] B. Tanatar and D. M. Ceperley, Phys. Rev. B **39**, 5005 (1989).
[5] D. M. Ceperley and B. J. Alder, Phys. Rev. Lett. **45**, 566 (1980).
[6] F. Rapisarda and G. Senatore Aust, J. Math. Phys. (N.Y.) **49**, 161 (1996)
[7] C. Attaccalite, S. Moroni, P. Gori-Giorgi, and G. B. Bachelet, Phys. Rev. Lett. **88**, 256601 (2002).
[8] Y. Kwon, D. M. Ceperley, and R. M. Martin, Phys. Rev. B **48**, 12037 (1993).
[9] B. Bernu, L. Cândido, and D. M. Ceperley. Phys. Rev. Lett. **86**, 870 (2001).
[10] B. Bernu and D. M. Ceperley, cond-mat/0310309.
[11] E. Y. Andrei, G. Deville, D. C. Glattli, and F. I. B. Williams, Phys. Rev. Lett. **60**, 2765 (1988).
[12] J. M. Kosterlitz and D. J. Thouless, J. Phys. C **6**, 1181 (1973); P. M. Platzman and H. Fukuyama, Phys. Rev. B **10**, 3150 (1974).
[13] B. I. Halperin and D. R. Nelson, Phys. Rev. Lett. **41**, 121 (1978).
[14] C. C. Grimes and G. Adams, Phys. Rev. Lett. **42**, 795 (1979); J. Tempere *et al.*, Eur. Phys. J. B **32**, 329 (2003); F. M. Peeters, Phys. Rev. B **30**, 159 (1984).
[15] A. F. Andreev and I. M. Lifshitz, Sov. Phys. JETP **29**, 1107 (1969).
[16] G. Katomeris, F. Selva, and J-L. Pichard, Eur. Phys. J. B **31**, 401 (2003); Z. A. Nemeth and J-L. Pichard, Eur. Phys. J. B **33**, 87 (2003).
[17] B. Spivak and S. Kivelson, Phys. Rev. B **70**, 155114 (2004).
[18] D. F. B. ten Haaf, H. J. M. van Bemmel, J. M. J. van Leeuven, W. van Saarlos, and D. M. Ceperley, Phys. Rev. B **51**, 13039 (1995).
[19] N. Trivedi and D. M. Ceperley, Phys. Rev. B **41**, 4552 (1990).
[20] D. M. Ceperley and M. H. Kalos, in *Monte Carlo Method in Statistical Physics*, edited by K. Binder (Springer-Verlag, Heidelberg, 1992).
[21] D. Ceperley, G. V. Chester, and M. H. Kalos, Phys. Rev. B **16**, 3081 (1997).
[22] S . Sorella, Phys. Rev. Lett. **80**, 4558 (1998).
[23] F. A. Stevens, Jr. and M. A. Pokrant, Phys. Rev. A **8**, 990 (1973).